Electron detachment from negative ions in a short laser pulse

Shearer, F., Smyth, M., & Gribakin, G. (2011). Electron detachment from negative ions in a short laser pulse. Physical Review A, 84(3), [033409]. DOI: 10.1103/PhysRevA.84.033409

Published in:
Physical Review A

Document Version:
Early version, also known as pre-print

Electron Detachment from Negative Ions in a Short Laser Pulse

†M.C. Smyth, S.F.C. Shearer G.F. Gribakin

Centre for Theoretical Atomic, Molecular and Optical Physics,

Queen's University Belfast, Belfast, BT7 1NN, UK and

†*Atomistic Simulation Centre, Queen's University Belfast, Belfast, BT7 1NN, UK**

We present an efficient and accurate model to study electron detachment from negative ions by a few-cycle linear laser pulse. In our calculations we modify the adiabatic model of Gribakin and Kuchiev [Phys Rev A **55**, 3760 (1997)] to calculate the transition amplitude of ionization for a short laser pulse. Application of the method of Gribakin and Kuchiev modified for a time-dependent short laser pulse with N optical cycles produces $2(N+1)$ saddle point contributions to the amplitude. Our calculations show that the inner N roots account for dominant contribution to the transition amplitude. We consider three intensities in our calculations, namely 10^{10} W/cm^2, 5×10^{10} W/cm^2 and 10^{11} W/cm^2. Detachment probabilities are considered for a range of intensities as well as phases. The dependence of the electron angular distribution on different initial phase shifts for different intensities are also considered, thus providing a new method for measuring the absolute phase of the pulse. An interference structure in the electron angular distributions is observed and accounted for correctly within our theory. Additionally our calculations predict that the behaviour of the energy spectra is both oscillatory and phase dependent. Finally results for the total detachment probability are also calculated.

PACS numbers: 32.80. Rm, 32.80.Gc, 32.80.Wr 32.80 Fb

I. INTRODUCTION

In this paper we extend the theory of Gribakin and Kuchiev [1] to describe the multi-

*Electronic address: f.shearer@qub.ac.uk

photon detachment of electrons from atomic negative ions for a short linear polarized laser pulse based on the Keldysh approximation [2]. The original theory of [1] formulated within the length gauge was developed to describe electron detachment in a periodic laser pulse from negative ions. In this approach the quantum mechanical transition amplitude of tunneling of a bound electron is given analytically by the contributions of two complex moments of time per period, calculated using the saddle point theory. One of the major outcomes of this work demonstrated that proper application of the Keldysh [2] approach to photodetachment allows one to make reliable quantitative predictions for total rates, energy spectra and angular distributions. The theory of Gribakin and Kuchiev [1] is now widely used by other researchers in the field. Application of the theory by [1] has been considered by Kuchiev and Ostrovosky [3] to consider negative ion detachment in a bichromatic laser field. Reichle et al [4] have experimentally verified that the theory of [1] successfully accounts for the predicted effect of quantum interference of electron trajectories in electron resolved angular distributions for the negative hydrogen ion. Further experimental evidence [5] supporting the strong field approximation of [1] is provided by a study of photodetachment of F^- in a strong linearly polarized pulse. This shows that [1] is qualitatively able to reproduce the energy and angle resolved spectrum without needing to incorporate the rescattering mechanism.

Recently in the literature there has been some disagreement between [6], and [7] over whether the length or velocity gauge is best adopted within the strong field approximation theory. However it has been demonstrated experimentally by Bergues et al [8] and that the length gauge should be used in the description of the electron interaction with the laser field as used in the strong field approximation of [1]. Bergues et al [8] shows the velocity gauge predicts a different interference structure in the electron energy and angular distributions compared with the length gauge. Direct comparison of his measurements with the length gauge theory of [1] and the velocity gauge theory of [6] demonstrates that only the length gauge approximation within the strong field approximation correctly reproduces the experimental data. Previous studies in the literature also show that when only the leading order of the transition amplitude is retained the model within the length gauge give a more accurate description of strong field ionization [9], [10].

Recently there is growing interest in the study of strong-field ionization by a few-cycle laser pulses. Martiny and Madsen [11] considered the photodetachment of atomic hydrogen

using the theory of [1] to study the ellipicity dependence of the validity of the saddle point method in a short laser pulse. The aim of the present paper is to adapt the formalism of [1] to short pulses and investigate the dependence of the total probability rates, electron angular and energy distributions on the phase providing a new method for measuring the absolute phase of the pulse [12].

In our paper, we apply our theory to consider the photodetachment of the negative hydrogen ion by three different intense (10^{10} W/cm^2, 5×10^{10} W/cm^2 and 10^{11} W/cm^2) few-cycle 10.6 μm laser pulses. The plan of this paper is as follows. We begin in Sec. II with the presentation of the general theory for multiphoton electron detachment of negative ions in a short laser pulse. Sec. III we present our numerical calculations for electron detachment of H^- at 10.6 μm, for three field intensities, namely 10^{10} W/cm^2, 5×10^{10} W/cm^2 and 10^{11} W/cm^2. In this section we also discuss our results. Finally in Sec IV we give our conclusions. Atomic units are used throughout, unless otherwise stated.

II. THEORY

A. Basic equations

We now consider the detachment of valence electron from an atom or negative ion due to a few-cycle laser pulse. The laser field of the short pulse may be defined as

$$\mathbf{F(t)} = -\frac{\mathbf{dA}}{\mathbf{dt}}. \tag{1}$$

where

$$\mathbf{A}(t) = \frac{\mathbf{F}}{\omega} \sin^2\left(\frac{\omega t}{2N}\right) \sin(\omega t + \alpha). \tag{2}$$

Here N is the number of optical cycles, ω is the frequency of the laser pulse and α is the phase. A short laser pulse lasts for a finite, and considerably small amount of time and thus to gain an understanding of ionization process we consider the detachment probability. This contains all the information about the electron and is defined as,

$$dw = |A_{\mathbf{p}}|^2 \frac{d^3p}{(2\pi)^3}. \tag{3}$$

where $A_{\mathbf{p}}$ is the amplitude of ionization of the n photon detachment process. The amplitude is given by,

$$A_{\mathbf{p}} = -i \int_0^{\tau} \int_0^{\infty} \Psi_{\mathbf{p}} V_F(t) \Psi_0 d\mathbf{r} dt. \tag{4}$$

where $\tau = \frac{2\pi}{N}\omega$ is the length of the laser pulse. $\Psi_0(t) = e^{-iE_0 t}\Phi_0(\mathbf{r})$ is the initial wave function of the initial electron state in the atomic potential $U(\mathbf{r})$

$$\left[\frac{p^2}{2} + U(\mathbf{r})\right] \Phi_0(\mathbf{r}) = E_0 \Phi_0(\mathbf{r}). \tag{5}$$

The potential energy of the electron interaction with the laser field, $V_F(t)$, is,

$$V_F(t) = \mathbf{r} \cdot \mathbf{F}(t), \tag{6}$$

in the length gauge interation operator of the electron. Neglecting the influence of the atomic potential $U(\mathbf{r})$ on the detached electron the final state is represented by the Volkov state, given by

$$\psi_{\mathbf{p}} = \exp\left[i(\mathbf{p} + \mathbf{k}_t) \cdot \mathbf{r} - \frac{i}{2}\int^t (\mathbf{p} + \mathbf{k}_{t'})^2 dt'\right], \tag{7}$$

where $\mathbf{k}_t$ is the classical electron momentum due to the field,

$$\mathbf{k}_t = -\int^t \mathbf{F}(t')dt'. \tag{8}$$

It is assumed that the lower limit contribution in the integral is zero as if the integration is performed from $-\infty$ and the integrand is switched on adiabatically. Also, the minus here is present due to the fact that the electron charge is -1 in atomic units. The Volkov wave function satisfies the Schrodinger equation

$$i\frac{\partial \Psi_{\mathbf{p}}}{\partial t} = \left[-\frac{p^2}{2} + V_F(t)\right] \Psi_{\mathbf{p}}. \tag{9}$$

Taking the complex conjugates of equations (7) and (9) and $i\frac{\partial \Psi_0}{\partial t} = E_0 \Psi_0$ the amplitude in equation (3) becomes

$$A_{\mathbf{p}} = \int_0^{\tau} \left[E_0 - \frac{1}{2}(\mathbf{p} + \mathbf{k}_t)^2\right] \tilde{\Phi}(\mathbf{p} + \mathbf{k}_t) \exp\left[\frac{i}{2}\int^t (\mathbf{p} + \mathbf{k}_{t'})^2 dt' - iE_0 t\right] dt, \tag{10}$$

where $\tilde{\Phi}(\mathbf{p} + \mathbf{k}_t)$ is the Fourier transform of $\Phi_0(\mathbf{r})$ and

$$\tilde{\Phi}(\mathbf{p} + \mathbf{k}_t) = \int e^{-i(\mathbf{p}+\mathbf{k}_t)\cdot\mathbf{r}} \Phi_0(\mathbf{r}) d\mathbf{r}. \tag{11}$$

An analytic form of equation (11) may be found by considering the general asymptotic form of $\Phi_0(\mathbf{r})$ which is valid since ionization primarily occurs at large distances from the nucleus. This is given by,

$$\Phi_0(\mathbf{r}) = Br^{\nu-1}e^{\kappa r}Y_{lm}(\theta,\phi). \tag{12}$$

where $\nu = \frac{Z}{\kappa}$ is the charge of the atomic residue and B is an asymptotic parameter associated with the particular ion being studied. For the particular case of the negative hydrogen ion where $\nu = Z = 0$ equation 12 becomes

$$\Phi_0(\mathbf{r}) = B\frac{e^{\kappa r}}{r\sqrt{4\pi}}. \tag{13}$$

Substituting this back into equation (11) yields

$$\tilde{\Phi}(\mathbf{p}+\mathbf{k}_t) = B\int \frac{e^{-i(\mathbf{p}+\mathbf{k}_t)\cdot\mathbf{r}}e^{\kappa r}}{r\sqrt{4\pi}}d\mathbf{r}. \tag{14}$$

and integrating gives,

$$\tilde{\Phi}(\mathbf{p}+\mathbf{k}_t) = \frac{2\sqrt{\pi}B}{[(\mathbf{p}+\mathbf{k}_t)^2+\kappa^2]}.$$

Thus the ionization amplitude in equation (10) reduces to yield,

$$A_{\mathbf{p}} = 2\sqrt{\pi}B\int_0^\tau \exp\left[\frac{i}{2}\int^t(\mathbf{p}+\mathbf{k}_{t'})^2dt' - iE_0t\right]dt. \tag{15}$$

B. Transition amplitude for a few-cycle laser pulse

By considering the phase in the exponent of the length-form amplitude equation (15) it may be seen that the integral contains a rapidly oscillating phase factor $\exp(if(t))$ where

$$f(t) = \frac{1}{2}\int^t(\mathbf{p}+\mathbf{k}_t)^2dt' - E_0t, \tag{16}$$

is the classical action. The presence of this rapidly oscillating factor in the transition amplitude prompts the use of the standard saddle point method so that the transition amplitude may be approximated by

$$A_{\mathbf{p}} = \frac{-B\sqrt{2}\pi}{\sqrt{-if''(t_N)}}\exp[if(t_N)], \tag{17}$$

where the saddle points t_N are obtained by setting

$$f'(t) = \frac{1}{2}(\mathbf{p}+\mathbf{k_t})^2 - E_0 = 0. \tag{18}$$

Thus from equation (18) it it may be seen that for a short laser pulse the adiabatic electron transition to the final state with a drift momentum p will occur when the condition

$$\frac{1}{2}\left(\mathbf{p}+\frac{\mathbf{F}}{\omega}\sin^2\left(\frac{\omega t}{2N}\right)\sin(\omega t_N+\alpha)\right)^2=E_0, \tag{19}$$

is satisfied. Solution of this equation yields the saddle point positions in the complex plane. By evaluating the classical electron momentum using equations (1), (2) and (8) and changing the integration variable ωt to ϕ_μ the saddle point equation (19) may be given explicitly as

$$f'(\phi_\mu)=p^2+\frac{2pF\cos\theta}{\omega}\sin^2\left(\frac{\phi_\mu}{2N}\right)\sin(\phi_\mu+\alpha)+\frac{F^2}{\omega^2}\sin^4\left(\frac{\phi_\mu}{2N}\right)\sin(\phi_\mu+\alpha)+\kappa^2=0, \tag{20}$$

where θ is the angle between the photoelectron momentum $\mathbf{p}$ and the field $\mathbf{F}$. The solution of this saddle point equation for a few cycle laser pulses necessitates a numerical approach. In section 3 we show that numerical solution of equation (19) reveals $2(N+1)$ complex saddle points which physically represent the emission of photoelectrons at various complex moments of time. This is a significant difference compared to the case of the long periodic pulse considered by Gribakin and Kuchiev [1], in which the saddle point equation could be solved anaytically. It is important to note that solutions to the saddle point equation are normally complex because ionization is a classically forbidden process except in the case of the over barrier regime. In [1] for the linearly polarized long pulse the saddle point equation yielded two pairs of complex conjugate saddle points, two of which were in the upper half complex plane and two in the lower half of the complex plane. However according to the general theory of adiabatic transitions [13] the saddle points in the lower half of the complex plane may be neglected. Thus the transition amplitude of ionization for a long periodic pulse may be obtained by summing over the two saddle points in the upper half of the complex plane. Physically the two saddle points describe complex moments of time per period corresponding to the maximum electric field strength. In the case of the short pulse however the number of saddle points depends on the number of optical cycles N and in calculating the transition amplitude we take into account only those saddle points that lie in the upper half of the complex plane. We show numerically in the next section that the amplitude for an N cycle pulse is given by

$$A_{\mathbf{p}}=\sum_{N=1}^{2(N+1)}\frac{-B\sqrt{2}\pi}{\sqrt{-if''(t_N)}}\exp[if(t_N)], \tag{21}$$

with $f(t_N)$ and $f''(t_N)$ evaluated for each of the $2(N+1)$ saddle point solutions of equation (20). To obtain the final form for the transition amplitude given by (21) we need explicit expressions for $f(t_N)$ and $f''(t_N)$ for the short laser pulse as described by equations (1) and (2). These are given in Appendix A.

III. NUMERICAL RESULTS AND DISCUSSION

In this section we apply the formulae obtained within the adiabtic theory to consider the photodetachment of H^-. To apply our theory to the case of H^- we require numerical values for the asymptotic parameters B and κ of the corresponding initial bound-state wave functions. The value of B is obtained from [15]. The values of κ are calculated from the corresponding binding energies $\kappa = \sqrt{(2|E_0|)}$ using Ref. [16]. In our calculations we have assumed a laser pulse with $N = 5$ optical cycles. We consider three short pulse intensities of 10^{10} W/cm^2, 5×10^{10} W/cm^2 and 10^{11} W/cm^2 each for phase shifts of $\alpha = 0, \pi/4$ and $\pi/2$. The saddle points in each case are initially obtained by considering the 3D surface plots of $\frac{1}{\sqrt{|f'(\phi)|}}$ so that the roots of the saddle point are visualized as 'infinities' rather than 'zeros'. The surface plots in each of the three intensities considered for each of the phases $\alpha = 0, \pi/4, \pi/2$ give twelve saddle points for the graphical solution of the saddle point equation. Thus we note that for our $N(= 5)$ cycle pulse we obtain $2(N + 1)$ saddle points. This result is in agreement with [11].

The approximate roots found from the graphical solution can be improved to yield more accurate approximations to the actual roots by using the Newton Raphson method for complex roots. The numerical calculation involves refining each root in turn, simultanaeously over a range of the angles θ between the direction of the laser field and the momentum $\mathbf{p}$ of the detached electron. In the present calculations the range used for θ is $0 < \theta < 180^0$ taking a stepsize of 1^0. The range of values used for the momentum is determined from the total energy of the detached electron assumed to be 10 ω. In our calculations we use a 10.6 μm CO_2 laser pulse which corresponds to a laser frequency $\omega = 0.0043$. Thus the momentum values of $\mathbf{p}$ range from 0.021 to 0.29 a.u. obtained by considering $\mathbf{p} = \sqrt{(2\omega)}$ with equally spaced energy points $\epsilon_j = \omega_j/20$ and in our calculations we have taken j=1,2,...200.

A. Saddle point smiles

Figure 1 illustrates the twelve roots of the saddle point equation for three field intensities $I = 10^{10}$, $5{\times}10^{10}$ and 10^{11} W/cm^2 and phases of $\alpha = 0, \pi/4$ and $\pi/2$. For each root in each of the nine panels in Figure 1 a change in momentum p and angle θ is illustrated. Each root of the saddle point equation is represented by a 'cluster' of stars. where each 'cluster' of stars includes a root for the range of θ = 0,45, 90,135 and 180 and momenta $p = \omega_j/20$ for $j = 0, 50, 100, 150, 200$. Here θ is represented horiztonlly within each 'cluster' of stars and momenta is by the varying colours of stars, for each root. In the first row of Figure 1 the saddle points for each of the three intensities have been calculated with a phase of α =0, in the second row with $\alpha = \pi/4$ and in the third row with $\alpha = \pi/2$ respectively. It may also be observed that for each intensity and phase considered here that the clusters distribute themselves qualitatively in the shape of a smile with the first cluster of stars on the left handside of each smile being the first root and the last cluster on the right hand side being the twelfth root respectively. The twelve saddle points which lie in the comple plane of t, corresponds to the twelve instants at which electron detachment takes place. In each of the three rows of Figure 1 we see that as the intensity of the laser field increases the saddle points move closer towards the real axis. Additional calculations carried out (not shown here) to make a comparison with the long laser pulse considered in [1] depict a similiar pattern of saddle point behaviour versus laser field intensity observed in Figure 1. Our results in Figure 1 also show that the saddle points in each of the cases considered move away from the real axis with increasing momentum. This indicates it is more difficult for the short laser pulse to kick out the electron at higher momentum.

Having found the twelve saddle points for the short laser pulse for the case of $N = 5$ optical cycles we now need to obtain the final expression for the transition amplitude for the short laser pulse. This involves substituting these roots back equation (21) and summing over all twelve saddle points.

B. Contribution of different saddle points to the detachment probability

In this section we calculate the probability distributions using the equation,

$$dw = \int_0^{\pi} \int_0^{\infty} |A_{\mathbf{p}}|^2 \frac{p d\varepsilon d\Omega}{(2\pi)^3}, \tag{22}$$

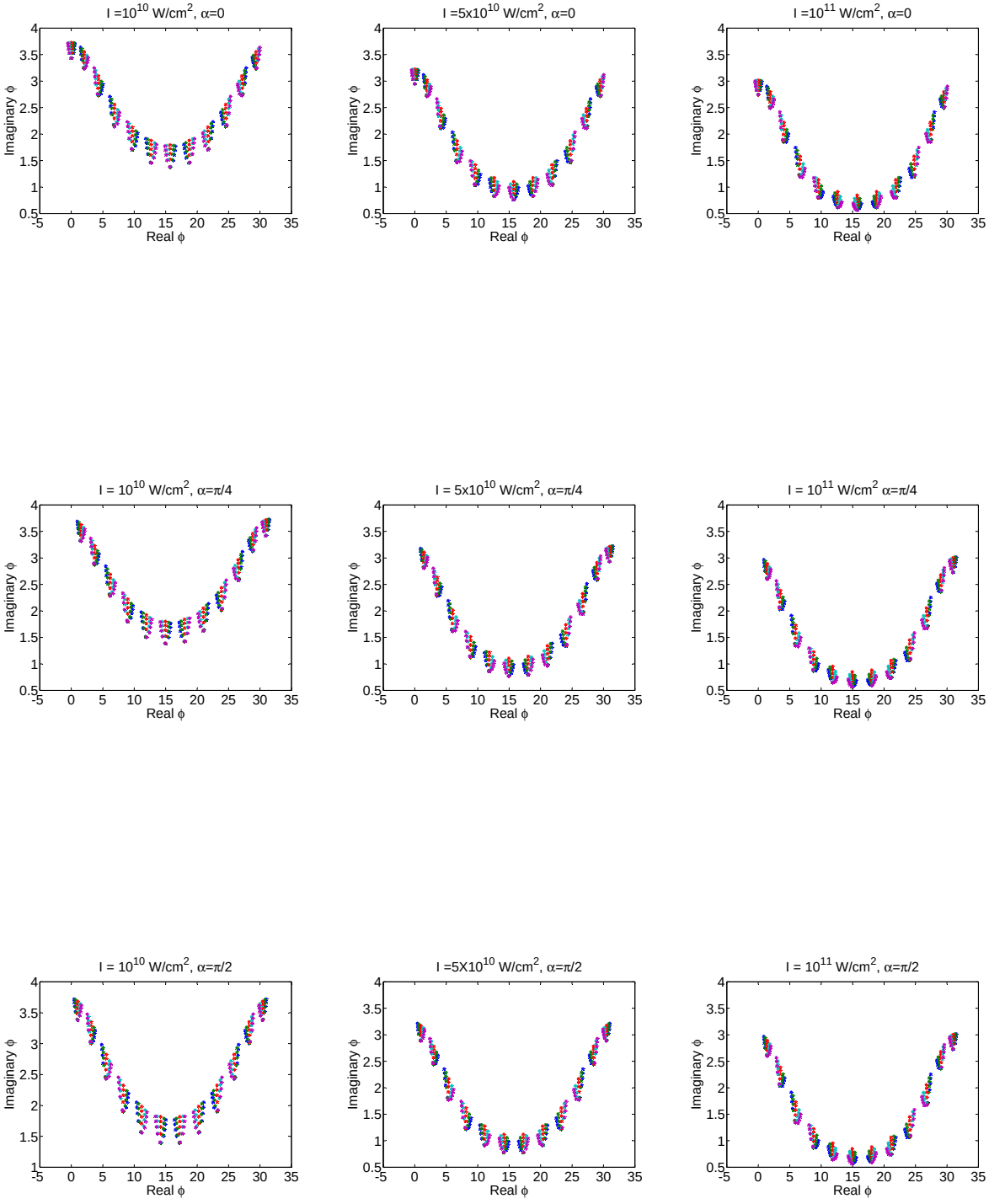

FIG. 1: Saddle points for the 12 twelve roots. Rows show increasing intensity 10^{10}, 5×10^{10} and 10^{11}W/cm^2. Columns show increasing phase shifts, 0, $\alpha = \frac{\pi}{4}$ and $\frac{\pi}{2}$.

where,

$$\frac{dw}{d\varepsilon d\Omega} = \frac{|A_{\mathbf{p}}|^2 p}{(2\pi)^3}. \tag{23}$$

In [1] detachment rates were considered since a long laser pulse is both regular and periodic. In a long pulse the behaviour of the system is evaluated over one cycle and applied to the rest of the pulse. However in a short laser pulse, there are few cycles and so each cycle must be considered separately. Hence here we need to consider detachment probabilities instead of detachment rates.

The rows of Figure 2 show the total detachment probabilities obtained by including different numbers of contributory saddle points in the transition amplitude. The columns in Figure 2 show the detachment probabilities for the three increasing field intensities 10^{10} W/cm^2, 5×10^{10} W^2 and 10^{11} W/cm^2. Each panel also depicts a range of θ and energy ϵ of the detached electron for the same phase shift of $\alpha = 0$. Also, it should be noted that this detachment probability must again be multiplied by 2 in order to take into account the two electrons in the Hydrogen negative ion. Considering the first row of Figure 1 with the lowest intensity of $I = 10^{10}$ W/cm^2 it is clear that there is a very small probability that the electron will be detached with a high energy. This may be noted from the large flat area in each of the frames of row 1. Next considering row 2 and 3 we see that the probability of the electron detaching at a high energy increases with increasing field intensity. This result indicates that at higher intensities it is easier for the laser pulse to detach an electron with a higher energy. We also note that by comparing the first panel in each column with the second panel in each column that the main contribution to total detachment probability comes from the middle five saddle points, which are the fifth, sixth, seventh, eighth and ninth saddle points. That is neglecting the contributions of the seven outer saddle points (i.e the first, second, third, located on the lefthand side of the smiles as shown in Figure 1 and the fourth, tenth, eleventh and twelfth, located on the righthand side of the smiles as shown in Figure 1 respectively) does not affect the magnitude of the detachment probability. This result is true for each of the intensities considered. By considering each panel in the second column with each panel in the third column we see that the fifth and ninth saddle points make a dominant contribution to the detachment probability. That is the saddle points which are closest to the real axis influence the behaviour of the ionisation amplitude. These results also indicate that it is more difficult for the short

laser pulse to kick the electron out at higher and this is supported by our simulations in 2 and table 1 below which show that the probability of electron detachment occuring at the first, second, third, fourth, tenth, eleventh and twelfth saddle points is extremely low.

Table 1 shows the total detachment probabilities obtained by including various saddle point contributions with a phase shift $\alpha = 0$ for the three field intensities. For $I = 10^{10}$ W/cm^2 it may be seen that the contributions from the fifth-ninth saddle points gives a larger ionization probability than the contribution from all twelve roots. This suggests that there are some interference effects at this intensity and phase corssponding to the coherent detachment of electrons at different instants of time. We also observe that the contribution from the sixth to the eighth saddle point contribute 94.65% of the detachment probability. In the case of $I = 5{\times}10^{10}$ W/cm^2 it can be seen that roots fifth to the ninth saddle points give a 99.84% contribution to the final detachment pronbability and we note an interefence effect for the saddle point contribution from the sixth to the eight roots. Finally in the case of $I = 10^{11}$ W/cm^2 it may be seen that the contribution from the fifth-ninth saddle points make up to 94% of the ionisation probability. Again we note an interference effect caused due to the contribution of the sixth to the eight saddle points. These results confirm our graphical results that it is the saddle points closest to the real axis that contribute most to the ionisation amplitude. Our results suggest the crude result that for an N cycle pulse the N middle saddle point roots closest to the real axis will yield the near total probability of detachment. Furthermore our results in this section also show that the adiabatic theory described for the short laser pulse accurately predicts the nature of the structure of the detachment probabilities as a result of interference caused by the electrons being detached at different instants of time.

Our simulations in Figure 2 show the detachment probabilities calculated with the inclusion of all twelve saddle points for the three sets of intensities varying intensities and phases $\alpha = 0, \pi/4$ and $\pi/2$. For the case of $I = 10^{10}$ W/cm^2 in the first row of Figure 3 we can see that the first peak at 180^0 gives a smaller value of detachment probability as the phase shift is increased in frames 2 and 3.Considering $I = 5 \times 10^{10}$ w/cm^2 and $I = 10^{11}$ we observe that the distributions for $\alpha = \pi/4$ and $\pi/2$ become asymmetric. It can be seen from the all the frames in Figure 3 that as the intensity increases the probability of detachment

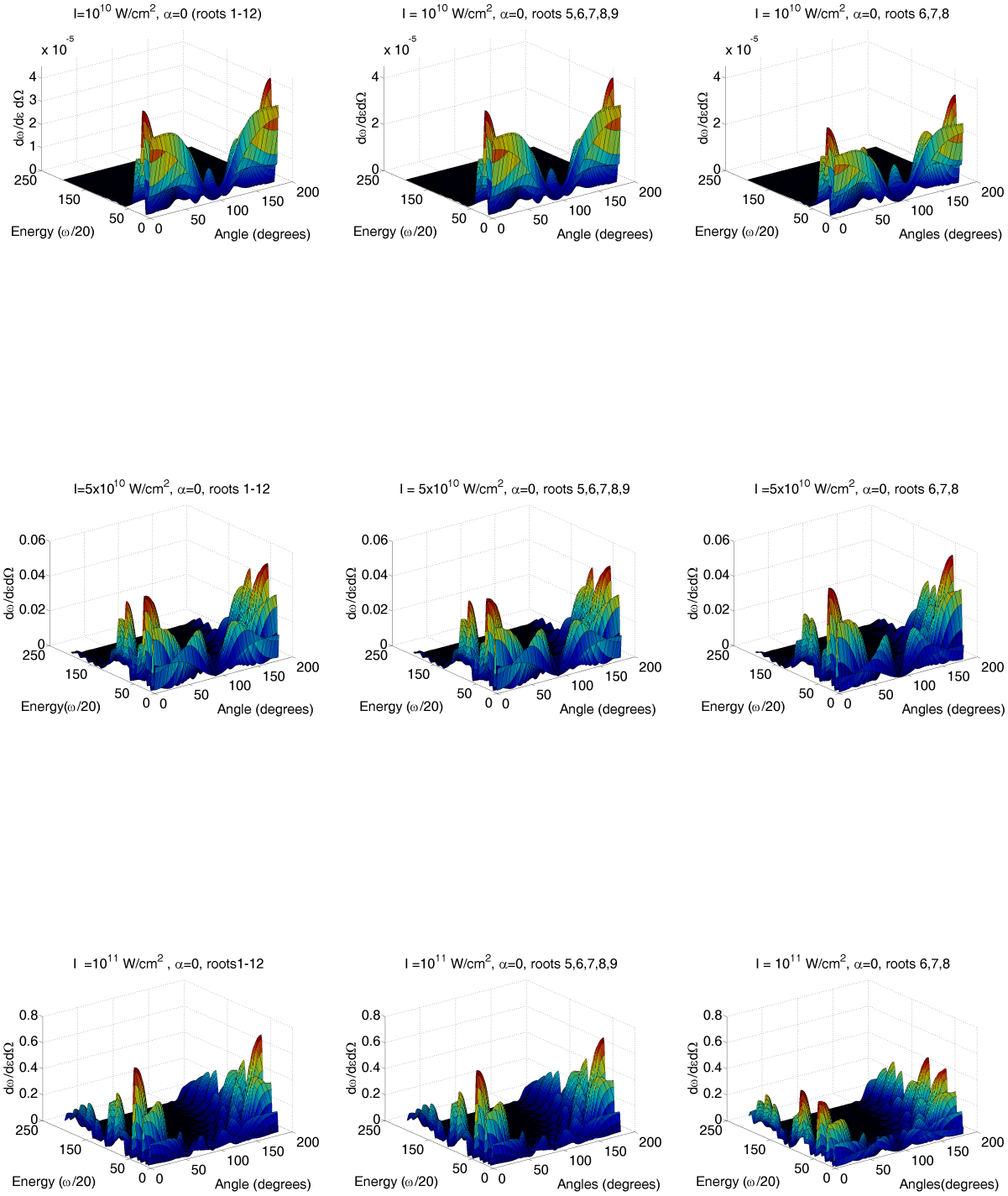

FIG. 2: Detachment Probabilities $d\omega/d\Omega d\epsilon$ for phase shift $\alpha = 0$. Rows show detachment probabilities calculated with contribution from all 12 saddle points, the middle five (5,6,7,8,9) saddle points and the middle three (6,7,8) saddle points respectively. The columns show the detachment probabilities calculated for increasing intensities of $I = 10^{10}\mathrm{W/cm^2}$, $I = 5 \times 10^{10}\mathrm{W/cm^2}$ and $I = 10^{11}\mathrm{W/cm^2}$ respectively. The Y axis shows energy in step sizes of $\frac{\omega}{20}$.

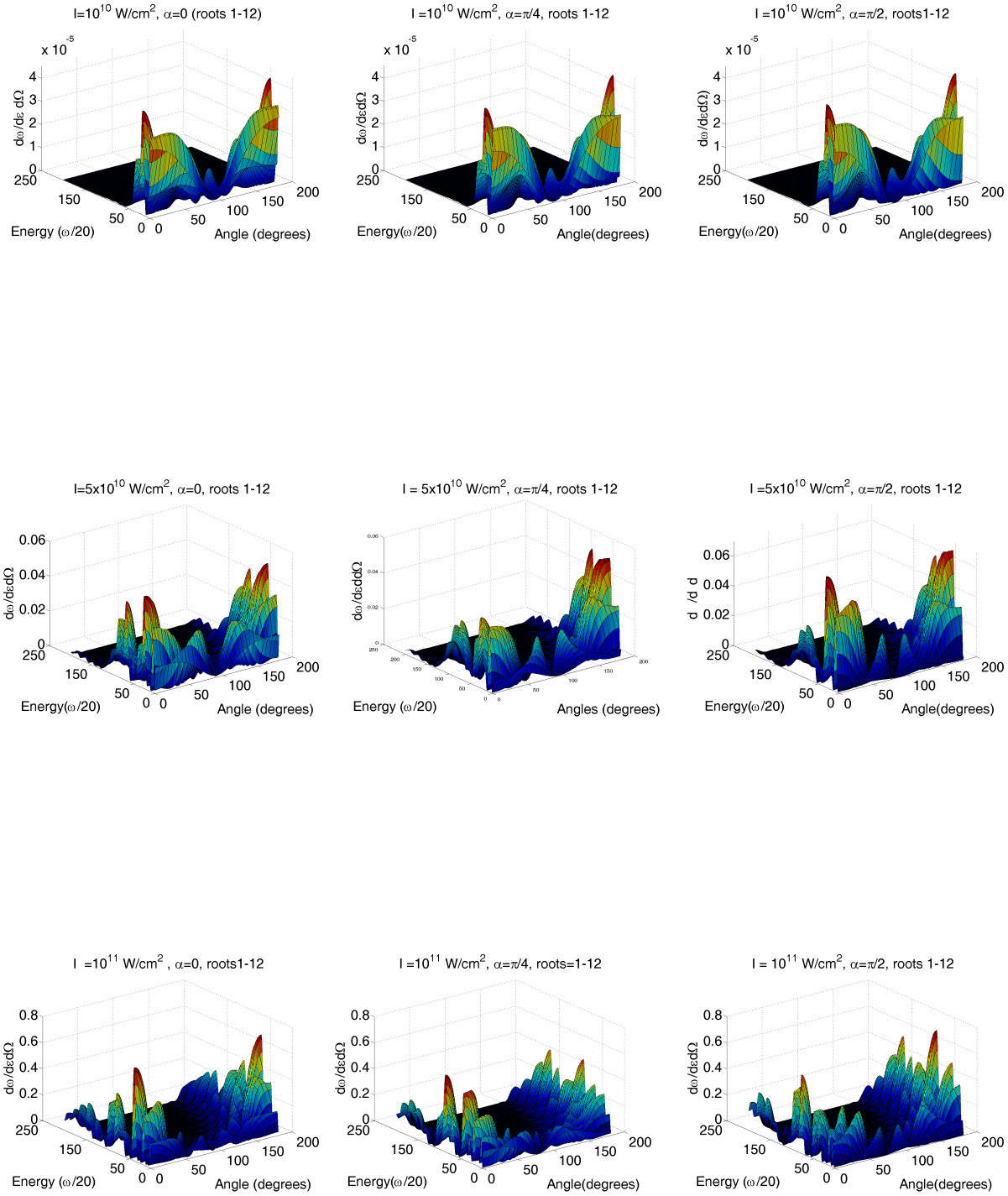

FIG. 3: Detachment Probabilities $d\omega/d\Omega d\epsilon$ calculated with contribution from all tweleve saddle points. Rows show detachment probabilities calculated with increasing phase shift $\alpha = 0$, $\alpha = \pi/4$ and $\alpha = \pi/2$ respectively. The columns show the detachment probabilities calculated for increasing intensities of $I = 10^{10}\mathrm{W/cm^2}$, $I = 5 \times 10^{10}\mathrm{W/cm^2}$ and $I = 10^{11}\mathrm{W/cm^2}$ respectively. The Y axis shows energy in step sizes of $\frac{\omega}{20}$.

Number of roots	Total detachment probabilities calculated for α=0		
Roots	$I = 10^{10}$	$I = 5 \times 10^{10}$	$I = 10^{11}$
$1 - 12$	1.1901×10^{-14}	6.9278×10^{-8}	1.3084×10^{-5}
$5 - 9$	1.1903×10^{-14}	6.9167×10^{-8}	1.2309×10^{-5}
$6 - 8$	1.1266×10^{-14}	7.6491×10^{-8}	1.6890×10^{-5}

TABLE I: Multiphoton detachment spectra of H^- in the strong $C0_2$ laser field with ω=0.0043. The total detachment probabilities are calulated by equation (26) with $B = 0.75$ and $\kappa = 0.235$ for intensities 10^{10}W/cm^2, 5×10^{10}W/cm^2 and 10^{11}W/cm^2 with a phase shift $\alpha = 0$. The total detachment probabilities have been calculated considering the contribution from all twelve saddle points, the middle five (5,6,7,8,9) saddle points and the middle three (6,7,8) saddle points respectively.

increases. These results are confimed in Table 2.

The absolute values of the 5 cycle laser pulse detachment cross sections are shown in Table 2 for the three field intensitiea calculated at the phase shifts $\alpha = 0, \pi/4$ and $\pi/2$. We note that for each intensity the detachment probability increases as the phase shift α is increased. This suggests that the detachment probability is phase dependent. This phase dependence may be caused by the imaginary parts of the transition amplitude resulting from from saddle point contributions.

C. Angular Dependance on Initial Phases

The angular dependence of the electron detachment due to the different initial phase shifts is shown in Figure 4. Here a slice of the 3d graphs from Figure 3 were taken as these surface plots include the contribution of all twelve saddle points in the evaluation of the transition amplitude. For each intensity, the detachment energy was chosen to correspond

Phase shift	Total detachment probabilities		
α	$I = 10^{10}$	$I = 5 \times 10^{10}$	$I = 10^{11}$
0	1.1901×10^{-14}	6.9278×10^{-8}	1.3084×10^{-5}
$\pi/4$	1.2038×10^{-14}	9.7566×10^{-8}	1.3276×10^{-5}
$\pi/2$	1.2175×10^{-14}	1.2722×10^{-7}	1.4337×10^{-5}

TABLE II: Multiphoton detachment spectra of H^- in the strong $C0_2$ laser field with ω=0.0043. The total detachment probabilities are calulated by equation (26) with $B = 0.75$ and $\kappa = 0.235$ for intensities 10^{10}W/cm^2, 5×10^{10}W/cm^2 and 10^{11}W/cm^2 with phase shifts $\alpha = 0$, $\alpha = \pi/4$ and $\alpha = \pi/2$ respectively. The total detachment probabilities in each case have been calculated considering the contribution from all twelve saddle points.

with the most likely probability of ionisation, and the detachment probbaility plotted against θ.

From the graphs it is evident that at the lowest intensity altering the phase shift has very little effect on the detachment probability. Here the detachment energy in units of $\omega/20$ was 20. In the second frame of Figure 4 we see that as the intensity is increased to $5\times$ 10^{10} W/cm^2 that increasing the phase shift has a more marked effect of the magnitude of the detachment probability. In this case it appears that the trend is the lower the phase shift the higher the detachment probability for angles up to about 110^0 degrees and for angles between 110^0 and 180^0 the trend reverses. Here the detachment energy was 25 in units of $\omega/20$. In the third case where I=10^{11} W/cm^2 with a detachment energy chosen at 20 in units of $\omega/20$, we observe that the lower phase shifts result in higher detachment probabilities over a wide range of angles. It is also noted that the detachment probability is clearly symmetric over all angles for all intensities considered. We also observe that the likelihood of detachment is also increased with increasing intensity.

D. Energy Spectrum

Here we consider the energy spectrum which is given by the equation

$$\frac{dw}{d\varepsilon} = \int_0^{\pi} \frac{|A_{\mathbf{p}}|^2}{(2\pi)^2}\sqrt{2\varepsilon}\sin\theta d\theta. \tag{24}$$

The energy spectra are shown in Figure 5 and 6. In Figure 5 we show the behaviour of the energy spectra with various contributions of the saddle points considered within the transition amplitude. It can be seen from all three graphs that it is the central fifth, sixth, seventh, eighth and ninth saddle ponts that dominate the behavior of the energy spectra for all three intensities considered. This confirms our earlier results from the 3d surface plots considered in Figure 3. The graphs also show that the fifth and ninth saddle points make a significant contribution to the spectra giving indistinguishable results from including all twelve saddle points in the calculation.

In Figure 6 one of the most noticeable features of each of the figures is the presence of the peaks. These may result from the emission of the electron following the absorption of different number of photons. Since the photons in the short pulse are not mono-energetic, (that is, their energies are not certain, $\Delta\omega \sim \frac{1}{\tau} = \frac{\omega}{N}$), the peaks are broadened in comparison with the long pulse table 1 of [1], which illustrates the detachment probability for the absorption of 'n' photons. We also observe that these peaks are also a signature of Figure 6. In order to fully explain the energy spectrum of the electron detachment due the initial phase shift, it is useful to illustrate the graphs showing the electric field for the two main initial phases. Recalling that the field is given by equations (1) and (2) we illustrate the field for the two cases of $\alpha = 0$ and $\alpha = \pi/2$ in Figure III D.

Here it may be seen that the initial phase $\alpha = 0$ has one maximal cycle in the middle of the pulse. In the graph for the initial phase $\alpha = \frac{\pi}{2}$, it appears that the graph has a maximum and minimum cycle of equal size in the middle of the pulse, yet both these cycles are slightly smaller than the maximal cycle of the $\alpha = 0$ pulse. This can help explain the difference observed in Figure 6. Our results show that in general, $\alpha = \frac{\pi}{2}$ gives a smaller overall detachment probability than $\alpha = 0$. This may be related to the fact that the maximum field strength for $\alpha = \frac{\pi}{2}$ is smaller than for $\alpha = 0$, as illustrated in Figure 2. This observation is in agreement with the results reported for varying the phase shift to examine trends in the behaviour of angular dependence plotted against the overall detachment probabilities in the last section.

E. Total Detachment Probability

IV. CONCLUSION

In conclusion we have extended the adiabatic model of Gribakin and Kuchiev [1] to describe electron detachment from negative ions for a short pulse. In this approach we our calculations we have found that for a linear polarized pulse with N cycles we obtain $2(N+1)$ sadddle point contributions to the transition amplitude. Our theory also shows that the N inner saddle points dominates the behaviour of the transition amplitude. The detachment probabilities show three main features. Firstly they have a strong dependence on the dominant saddle point contributions, secondly they are highly asymmetric and thirdly they are influenced significantly by the phase shift between the pulse envelope and its carrier frequency. Our theory predicts an interference structure and a phase dependence in both the photoelectron angular distributions and energy spectra. In particular we can predict with accuracy the actual saddle points that cause the interference between the electrons emitted at various complex moments of time. The dependence of the electron angular distribution on the phase shift provides a new method for measuring the absolute phase of the pulse. Finally the findings of this work allow a qualitative and quantitative physical analysis of the problem of electron detachment from negative ions in a short laser pulse and may be of use to experimentalists.

Acknowledgments

APPENDIX: CALCULATION OF THE TRANSITION AMPLITUDE FOR A SHORT LASER PULSE

The transition amplitude for the short laser pulse may be calulated using the using the theory of Section II as

$$A_{\mathbf{p}} = \frac{-B\sqrt{2}\pi}{\sqrt{-if''(t)}} \exp[if(t)], \tag{25}$$

For multiphoton processes the integral over time in the transition amplitude contains the coordinate independent part of the classical action given by

$$f(t) = \frac{1}{2}\int^{t} (\mathbf{p}+\mathbf{k}_t)^2 dt' - E_0 t, \tag{26}$$

where $\mathbf{p}$ is the photoelectron momentum and the classical electron momentum $\mathbf{k_t}$ due to the

few-cycle pulse is given as

$$\mathbf{k_t} = \frac{\mathbf{F}}{\omega}\sin^2\left(\frac{\omega t}{2N}\right)\sin(\omega t+\alpha). \tag{27}$$

After some routine but heavy algebra the explicit form of the classical action for the short laser pulse is where θ is the angle between the photoelectron momentum $\mathbf{p}$ and the field $\mathbf{F}$. After some routine heavy algebra $f(t)$ given by equation (26) gives,

$$\begin{aligned}\int (p^2+2\mathbf{p}\mathbf{k}_{t'}+k_{t'}^2)\,dt' - E_0 t = \frac{1}{2}p^2 t - \frac{\mathbf{pF}}{2\omega}\cos(\omega t+\alpha) + \frac{\mathbf{pF}N}{4(N+1)\omega}\cos\left(\frac{N+1}{N}\omega t+\alpha\right)\\ +\frac{\mathbf{pF}N}{4(N-1)\omega}\cos\left(\frac{1-N}{N}\omega t-\alpha\right) + \frac{3tF^2}{32\omega^2} - \frac{4F^2N}{32\omega^3}\sin\left(\frac{\omega t}{N}\right) + \frac{F^2N}{64\omega^3}\sin\left(\frac{2\omega t}{N}\right)\\ -\frac{3F^2}{64\omega^3}\sin(2\omega t+2\alpha) + \frac{2NF^2}{32(1-2N)\omega^3}\sin\left(\frac{(1-2N)}{N}\omega t-2\alpha\right)\\ +\frac{2F^2N}{32(1+2N)\omega^3}\sin\left(\frac{(1+2N)}{N}\omega t+2\alpha\right) - \frac{NF^2}{128(1-N)\omega^3}\sin\left(\frac{2(1-N)}{N}\omega t-2\alpha\right)\\ -\frac{NF^2}{128(1+N)\omega^3}\sin\left(\frac{2(1+N)}{N}\omega t+2\alpha\right).\end{aligned} \tag{28}$$

where θ is the angle between the photoelectron momentum $\mathbf{p}$ and the field $\mathbf{F}$. In the above expression we have neglected the lower limit in the integration as this only adds a common phase factor to all saddle point contributions. Next we require $f''(t)$ and this is evaluated by considering

$$f''(t) = (\mathbf{p}+\mathbf{k}_t)\frac{d}{dt}\mathbf{k}_t \tag{29}$$

where

$$\frac{dk_t}{dt} = \mathbf{F}\omega\sin^2\left(\frac{\omega t}{2N}\right)\cos(\omega t+\alpha) + \frac{F\omega}{2N}\sin(\omega t+\alpha). \tag{30}$$

and substitution of equation (30) into (29) yields,

$$\begin{aligned}f''(t) = \frac{pF\cos\theta}{2\omega N}\sin\left(\frac{\omega t}{N}\right)\sin(\omega t+\alpha) + \frac{pF\cos\theta}{\omega}\sin^2\left(\frac{\omega t}{2N}\right)\cos(\omega t+\alpha)\\ +\frac{f^2}{2\omega^2 N}\sin\left(\frac{\omega t}{N}\right)\sin^2\left(\frac{\omega t}{2N}\right)\sin(\omega t+\alpha)^2 + \frac{f^2}{\omega^2}\sin^4\left(\frac{\omega t}{2N}\right)\cos(\omega t+\alpha)\sin(\omega t+\alpha).\end{aligned} \tag{31}$$

Finally substitution of $f(t)$ from equation (28) and $f''(t)$ from equation (31) into equation (25) gives the final expression for the transition amplitude.

---

[1] G.F. Gribakin and M. Yu. Kuchiev, Phys. Rev. A **55**, 3760 (1997).

[2] L. V. Keldysh, Zh. Eksp. Teor. Fiz. **47**, 1945 (1964) [Sov. Phys. JETP **20**, 1307 (1965)].

[3] M. Yu. Kuchiev and V.N. Ostrovsky, Phys. Rev. A **59**, 2844 (1999).

[4] R. Reichle, H. Helm, and I. Yu. Kiyan, Phys. Rev. Lett. **87**, 243001 (2001).

[5] I. Yu. Kiyan and H. Helm, Phys. Rev. Lett. **90**, 183001 (2003).

[6] H.R. Reiss, Phys. Rev. A, **77**, 067401, (2008).

[7] B. Bergues, Z. Ansari, D. Hanstorp and I. Yu. Kiyan, Phys. Rev. A,**77**, 067402, (2008).

[8] B. Bergues, Z. Ansari, D. Hanstorp and I.Yu. Kiyan, Phys. Rev. A**75**, 063415 (2007).

[9] T.K. Kjeldsen and L.B. Madsen J. Phys. B, **6**, 2033, (2004).

[10] D. Bauer, D.B. Milosevic and W. Becker, Phys. Rev. A, **72**, 023415, (2005).

[11] C. P. J. Martiny and L.B.Madsen, Phys. Rev. A **78**, (2008).

[12] X. Liu and C. Figueira de Morrison Faria, Phys. Rev. Lett. **90**, 183001, (2003).

[13] L. D. Landau and E. M. Lifshitz, *Quantum Mechanics. Non-relativitic Theory* (Peragmon, Oxford, 1965).

[14] B. M. Smirnov, *Physics of Atoms and Ions.* (Springer 2003).

[15] E.E. Nikitin and B.M. Smirnov, *Atomic and Molecular Processes* (Nauka, Moscow, 1988).

[16] H. Hotop and W.C. Lineberger, J. Phys. Chem. Ref. Data **14**, 731 (1985).

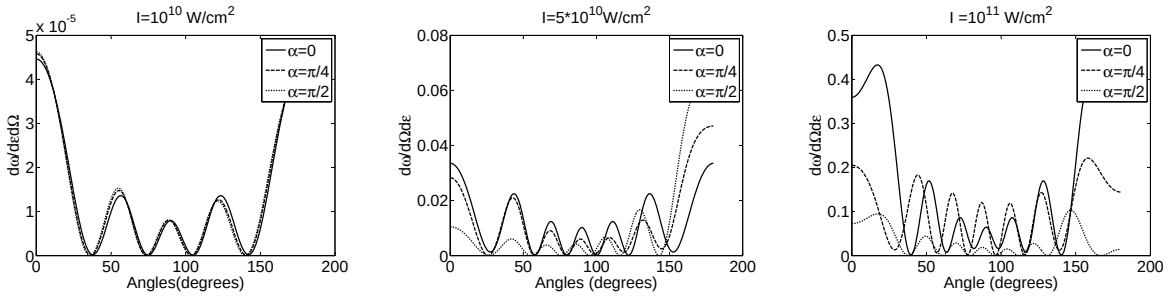

FIG. 4: Angular distributions calculated for the three intensities, $I = 10^{10}\mathrm{W/cm^2}$, $5 \times 10^{10}\mathrm{W/cm^2}$ and $10^{11}\mathrm{W/cm^2}$. The angular distributions show the effect of the phase shift at $\alpha = 0$, (solid line), $\pi/4$, (long dashed line) and $\pi/2$, (short dashed line) has on the detachment probability calculated at the peak in detachment energy in units of $\omega/20$ at energies of 20, 25 and 20 corresponding to intensities of 10^{10}, $5\times$ 10^{10} and 10^{11} $\mathrm{W/cm^2}$ respectively.

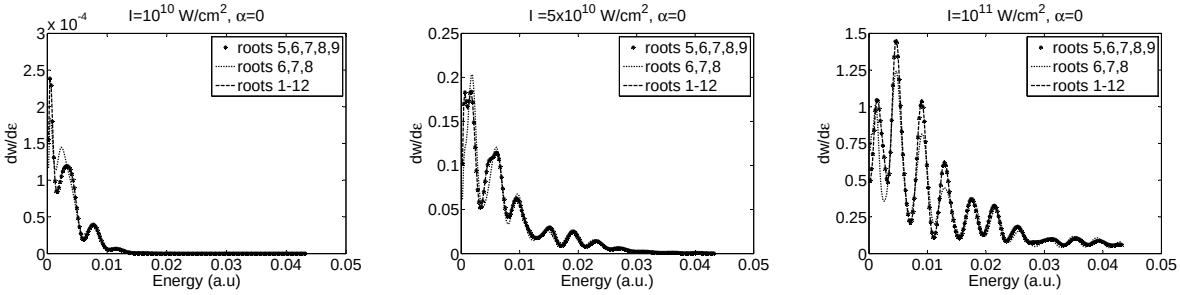

FIG. 5: Energy spectra(a) $I = 10^{10}\mathrm{W/cm^2}$ calculated with the contribution from the five cental saddle points namely 5,6,7,8 and 9: shown by stars, the three inner saddle points, namely 6,7,8: long dashed line and the 12 saddle points: short dashed line, (b) $I = 5 \times 10^{10}\mathrm{W/cm^2}$ calculated with the contribution from the five cental saddle points namely 5,6,7,8 and 9: shown by stars, the three inner saddle points, namely 6,7,8: long dashed line and the 12 saddle points: short dashed line (c) $I = 10^{11}\mathrm{W/cm^2}$ calculated with the contribution from the five cental saddle points namely 5,6,7,8 and 9: shown by stars, the three inner saddle points, namely 6,7,8: long dashed line and the 12 saddle points: short dashed line.

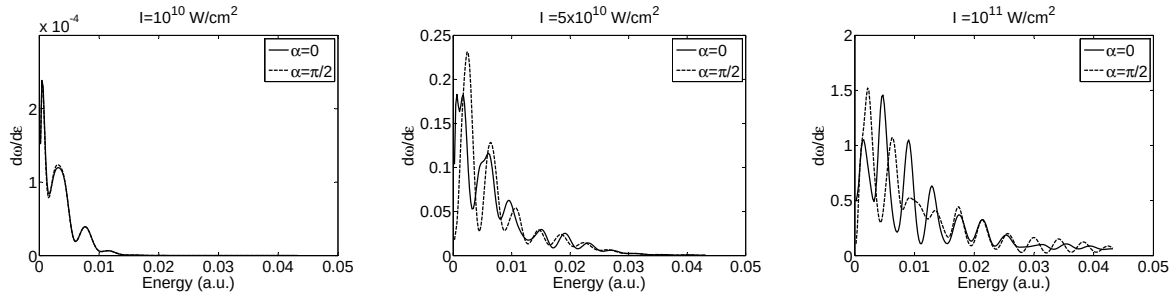

FIG. 6: Energy spectra(a) $I = 10^{10}\mathrm{W/cm^2}$ calculated with the a phase shift $\alpha = 0$: solid line and $\alpha = \pi/2$: long dashed line (b) $I = 5 \times 10^{10}\mathrm{W/cm^2}$ calculated with a phase shift of $\alpha = 0$: solid line and $\alpha = \pi/2$: long dashed line (c) $I = 10^{11}\mathrm{W/cm^2}$ calculated with a phase shift $\alpha = 0$: solid line and $\alpha = \pi/2$: long dashed line.

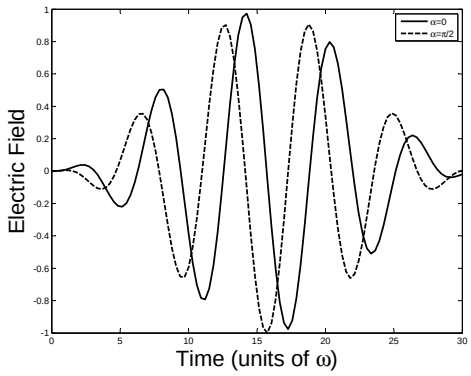

FIG. 7: Electric field for short pulse, with changing initial phase, $\alpha = 0$: solid line and $\frac{\pi}{2}$: long dashed line.